CrossMark

Influence of Laser Glazing on the Characterization of Plasma-Sprayed YSZ Coatings

Yan Wang[1] · Jiangwei Liu[1] · Hanlin Liao[1] · Geoffrey Darut[1] · Jorge Stella[3] · Thierry Poirier[2] · Marie-Pierre Planche[1]

Abstract In this study, 8 wt.% yttria-stabilized zirconia powder was deposited on the substrates by atmospheric plasma spray. The coatings were post-treated by laser glazing under different parameters in order to densify them. The characterization of the laser molten pools under different laser treatment conditions was studied. Preheating processes were also employed. Scanning electron microscopy observations of the surface and cross section of as-sprayed and laser-glazed coatings were carried out to investigate the influence of laser glazing on the microstructure on laser-glazed coatings. The results show that preheating processes improve the coating in terms of deepening the laser-glazed layer, reducing the number of vertical cracks and surface density of cracks and widening the molten pool. Finally, the influences of linear energy density on the characterization of the glazed layer are discussed.

Keywords APS · laser Glazing · laser molten pool · SEM observation · YSZ coating

✉ Yan Wang
   yan.wang@utbm.fr; wangyan140511@hotmail.com

1   UTBM, LERMPS, University of Bourgogne Franche-Comté, Belfort, France

2   Institut de Céramique Française, Limoges, France

3   Departamento de Ciencia de los Materiales, Universidad Simón Bolívar, Caracas, Venezuela

Introduction

8 wt.% yttria-stabilized zirconia (8YSZ) is mostly used to manufacture thermal barrier coating (TBC) as a ceramic layer (Ref 1, 2). TBC is widely applied to the combustion chamber of gas turbine engines, because the coating can provide high thermal gradient with cooling backside and hot outside. So it enables the gas turbine to work in relative high-temperature environment. Thus, it increases the thermal efficiency significantly (Ref 3). In addition, the stress-induced phase transformation from tetragonal phase to monoclinic phase in YSZ increases its fracture toughness for the protection against cavitation erosion (Ref 4). Moreover, YSZ material is also used in applications like solid oxide fuel cells (SOFC) and oxygen sensors for its advantages like adequate ionic conductivity, stability in dual environment especially (Ref 5), but the required microstructure is much denser than in TBC.

However, after plasma spraying, volume shrinkage and tensile stress on the top of the fabricated coating lead to crack networks on the surface of YSZ coatings. These cracks and pores are detrimental for mechanical properties. In addition, the oxidation of the bonding layer and the corrosion of the components lead together to the failure of TBCs (Ref 6). In the case of the SOFC application, plasma spraying induces pores which cause diffusion of fuel or air through the electrolyte (Ref 7). For all these reasons, it is necessary to heal and densify the coatings by post-treatment. Previous investigations have demonstrated that surface-sealing technique such as laser glazing could induce a denser top layer with reduced surface roughness, as well as cracks perpendicular to the surface (Ref 8-11). It is reported by Ahmadi-Pidani (Ref 12) that the life time of the laser-glazed TBCs is fourfold compared with the plasma-sprayed TBCs due to the strain accommodation through

induced segmented cracks. According to the study of Tsai (Ref 13), laser glazing could increase the life time of plasma-sprayed TBCs as long as four times when exposing to V_2O_5 salt-containing hot corrosion. Therefore, a laser glazing post-treatment is a useful way to heal and densify coatings (Ref 14-16).

The aim of present study is to densify the as-sprayed coating by laser remelting. Different parameters of laser treatment were adjusted to observe the influence of laser glazing on the microstructure of plasma-sprayed YSZ coating, particularly the effect of the pre-heating process.

Experimental Procedures

Preparation of the Coating Deposition

Commercial ZrO_2-8 wt.% Y_2O_3 powder (Plasmatex-powder) was employed as feedstock. Carbon steel disks were used as substrates with the specific dimensions of Ø25 × 9 mm. The substrates were first cleaned in an ultrasonic acetone bath during 10 min and second grit-blasted with alumina. A Sulzer-Metco F4 plasma gun was used to deposit 8YSZ coating. A plasma gas mixture composed of argon and hydrogen was employed. Argon was also employed as carrier gas. Table 1 illustrates the detail information of spraying parameters.

Laser Gazing Conditions

The post-laser treatment process was achieved by a Nd-YAG laser source designed by the Cheval company (Cheval, Pirey, France). This laser can supply a strong power with a maximum average power of 1100 W. The pulse duration can be adjusted from 0.5 to 10 ms. Wavelength and maximum frequency are 1064 nm and 200 Hz, respectively. Off-set distance is fixed to 340 mm, and the diameter of the spot is 3 mm at this focalization point.

During laser-glazing process, three factors were mainly used to control the linear density of laser energy, hence to get different microstructures and morphologies of the glazed coatings. They concern duration of laser firing pulse, the scanning speed and the energy density. The duration of each laser cycle is calculated from the ratio 1/F, F corresponding to a given frequency. The laser firing period is the heating time required by the laser during each cycle. In this model, it was assumed that the laser power is constant during each pulse as shown in Fig. 1. Table 2 depicts the parameters of the laser treatment. To evaluate the effect of laser parameters, ten unique tracks remelting were carried out with different scanning speeds, different durations for each fire pulse, and different intensities of the laser (the laser intensity of the imposed for varying the peak power laser). A calorimeter (Labmaster 4DOPTICAL USA) was used to measure the average power of the laser as defined by the following relationship:

$$P_a = P_p \tau \cdot F \qquad \text{(Eq 1)}$$

where P_a is its average power (W), P_p is the peak power (W), τ is the pulse duration of firing a pulse (ms) and F is its frequency (Hz).

Table 1 Spraying parameters

Parameters	Value
Electric arc current (A)	620
Electric arc voltage (V)	60
Plasma gas (NL/min)	Ar 32
	H_2 10
Carrier gas (NL/min)	3.5
Liner speed (m/s)	1.2
Stand-off distance (mm)	115
Substrate (mm)	Ø25 × 9
Powder	ZrO_2-8%Y_2O_3

Fig. 1 Powder morphology (a) and size distribution (b)
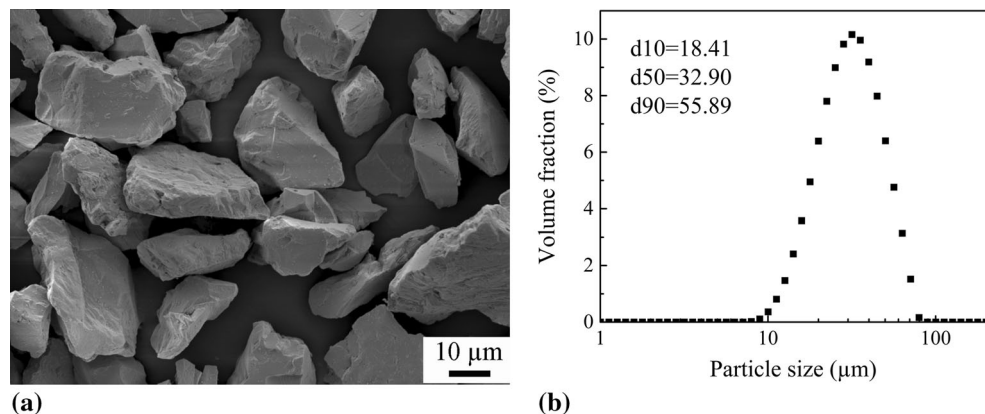
d10=18.41
d50=32.90
d90=55.89

(a) (b)

Table 2 Energy densities for different parameters

Case	Pulse duration (ms)	Velocity (mm/s)	Average power (W)	Peak power (W)	Energy density (J/cm^2)	Liner energy density (J/mm)
1	3	5	170	4700	332	28.2
2	4	5	261	6525	462	52.2
3	5	5	339	6780	480	67.8
4	6	5	424	7067	500	84.8
3	5	5	339	6780	480	67.8
5	5	10	339	6780	480	33.9
6	5	20	339	6780	480	16.95
7	5	30	339	6780	480	11.3
8	5	5	246	4920	348	49.2
3	5	5	339	6780	480	67.8
9	5	5	402	8060	570	80.60
10	5	5	486	9727	688	97.27

The laser power density follows the Gauss distribution and can be calculated by the following relationship:

$$\varphi(r) = \frac{P}{2\pi R^2} \exp\left(-\frac{r^2}{2R^2}\right) \qquad \text{(Eq 2)}$$

where P is the laser power (W) and R represents the dispersion radius of Gauss profile (1.5 mm), and r is the radial distance away from the center of the symmetry axis.

In addition, the as-sprayed coatings were pre-heated by 4, 8 and 12 laser passes with a spot of 10 mm and a scanning speed of 50 mm/s before laser glazing. Then, coatings were laser-glazed following the parameters matrix described in Table 2 varying the firing duration, the scanning speed and the energy density.

Characterizations of the Samples

Laser diffraction method (Maserter2000, Malvern, England) was used to measure the size distribution of the 8YSZ powder. Feedstock, coating cross and its surface morphology were characterized by scanning electron microscopy (SEM) and optical microscopy (OM). During the laser-glazing process, the temperature of the coatings was measured by infrared thermal imaging camera (SC 5210) developed by FLIR company.

Image J software was employed to estimate the porosity and the surface density of cracks. For the case of porosity tests, 10 SEM pictures were obtained at random places of polished cross sections at a magnification of 300. While with respect to surface density of cracks, firstly a threshold value was set to distinguish cracks from pores and dense areas in the coatings. Secondly, the pictures were converted to binary mode. Black pixels represent both cracks and pores, while white pixels corresponded to dense areas. Finally, the binary image was skeletonized in such a way
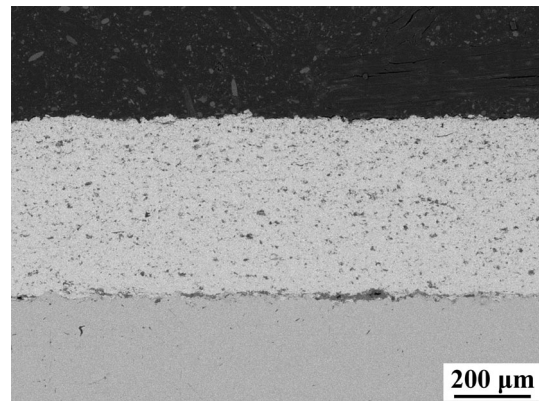

Fig. 2 Cross-sectional morphology of as-sprayed YSZ coating

that the width of cracks and pores was ignored. The black pixel lines were skeletonized as cracks. This way, the length of cracks could be estimated as the numbers of black pixels. The value of surface density of cracks is finally deduced from the ratio between the numbers of black pixels and the total number of pixels (Ref 17).

Results and Discussions

Characterization of the Feedstock Powder and the As-Sprayed Coatings

From the results shown in Fig. 1, average size of YSZ powder is 35.267 μm with d10 = 18.41 μm, d50 = 32.90 μm, d90 = 55.89 μm. Figure 2 displays the cross-sectional morphology of as-sprayed YSZ coating. It corresponds to a typical thermal spray structure with a porosity of 8.5 ± 1.2%. Figure 3 illustrates the surface temperatures of the coatings

by different preheating processes. Coatings were preheated to 285, 400 and 420 °C, respectively, before laser glazing.

Characterization of Laser-Glazed Coatings

Cross-sectional microstructure of laser-glazed coatings is shown in Fig. 4. The coatings exhibit a glazed layer with numerous vertical cracks. The quantity of the vertical cracks is much less for the preheated coating than for the one without preheating. Because the energy density of the laser spot is a Gaussian distribution (see Eq 2), the energy provides to the central area is higher than that to the border, on the contrary, the cooling rate is much higher for border areas compared to the central areas. Therefore, the solidification arises from the border to the central zone and induces tension stresses to the central areas due to the volume contraction. As a consequence, vertical cracks could be generated if the stress can not be released properly. As a result, Fig. 4(a) exhibits that a number of vertical cracks format to release stresses. Preheating process makes the temperature of the coating increasing to 420 °C,
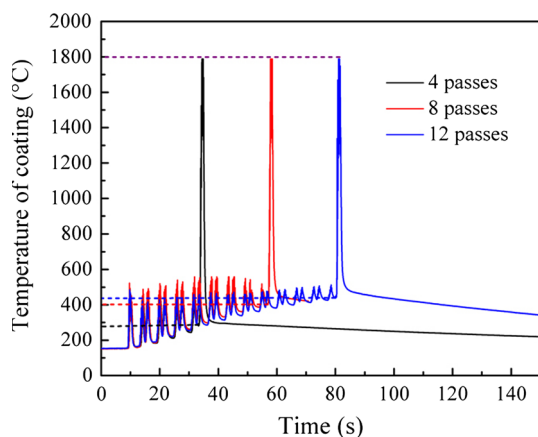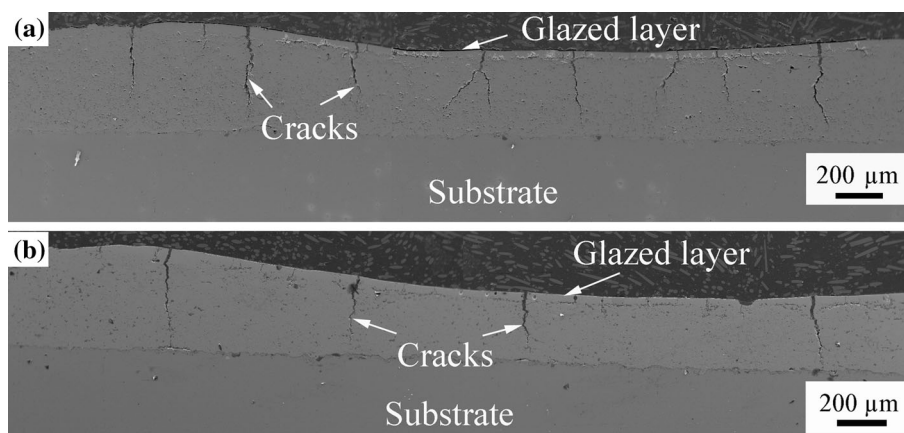
Fig. 3 Evolution of the coating temperature after 4, 8 and 12 passes preheating process

Inconsistent cooling rate between different areas is reduced. Hence, numbers of vertical cracks decreases significantly as can be observed in Fig. 4(b).

Through the cross-sectional microstructure of the laser-glazed coating (Fig. 5), two parts can be distinguished in the laser-glazed coating:

I.   A glazed layer locating on the top of the coating. This part exhibits a dense microstructure with few defects.

II. As-sprayed layer locating on the bottom of the coating

Comparing Fig. 5(a) with Fig. 5(b), it can be noted that the depth of glazed layer preheated to 420 °C is larger than that without preheating and the defects in the second zone are less numerous. After the preheating of coating, it could be supposed that the thermal gradient between molten layers and unmolten ones is small leading to reduce stresses caused by cooling rate. As a consequence, cracks in this specific zone are not needed to release stress Fig. 5(a).

Figure 6 illustrates surface crack nets in function of different process parameters. Cracks combine one with another in the whole surface of laser-glazed coating. While preheating is applied, the number of cracks decreases sharply as well as the width of cracks. The surface density of such cracks changes from 0.055 to 0.028 mm^{-1} (Fig. 7).

Linear Energy Density and Microstructure

During the laser-glazing process, different parameters (Table 2) are adjusted to get a proper microstructure. The influence of the linear energy density on the microstructure characteristics of laser-glazed coatings is visible.

Figure 8 displays the evolution of the length of the vertical cracks as a function of linear energy density. It can be observed that linear energy density does not influence the length of cracks very much. In fact, when the linear energy density increases from 11.3 to 97.3 J/mm, the
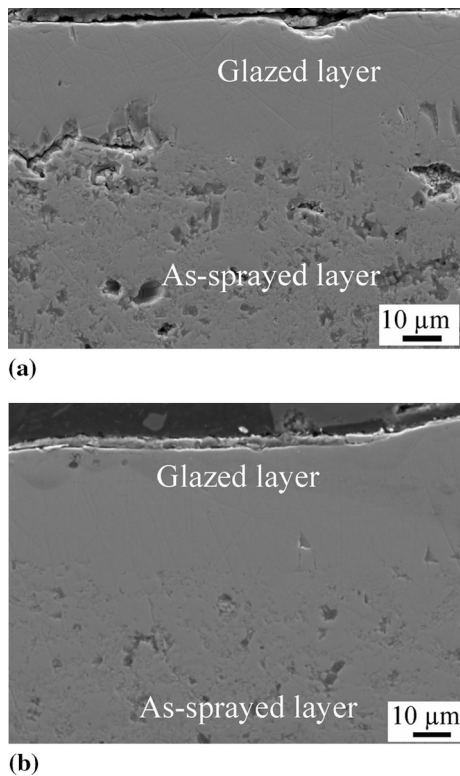
Fig. 4 Cross-sectional microstructure of laser-glazed coatings under parameters of case 3 (pulse duration: 5 ms, scanning speed: 5 mm/s and liner density of energy: 67.8 J/mm) without preheating (a), preheating to 420 °C (b)

Fig. 5 Close view of cross-sectional microstructure of laser-glazed coating under parameters case 3 (pulse duration: 5 ms, scanning speed: 5 mm/s and liner density of energy: 67.8 J/mm) without preheating (a), preheating to 420 °C (b)

Fig. 6 Surface morphology of laser-glazed coatings without preheating (a), preheated to 285 °C (b), 400 °C (c), and 420 °C (d) under parameters case 3 (pulse duration: 5 ms, scanning speed: 5 mm/s and liner density of energy: 67.8 J/mm)

length of vertical cracks varies from 194.5 to 316.7 μm. The corresponding results include two distinct stages:

i. At first, the length of cracks increases linearly with the increase in linear energy density.
ii. At second, the length of cracks still constant around 280 μm regardless of change of linear density. Also, the length of cracks of coating preheated does not differ from that without preheating.

The width of molten pool in function of different linear energy densities is also investigated. Increasing the linear energy density results in the linearly increase of width of molten pool as it is proved by the fitting function shown in Fig. 9, excepted for case 1. In this specific case, the duration of laser pulse is 3 ms and the linear density is 28.2 J/mm. Preheating processes also widen the molten pool. Indeed, width of molten pool increases from 4.42 to 5.1 mm as preheating temperature increases from 0 to 420 °C.

Figure 10 shows the relationship between depth of glazed layer and linear energy density. It seems that no evident correlation could be found between the two. Further investigation reveals that velocity, pulse duration and
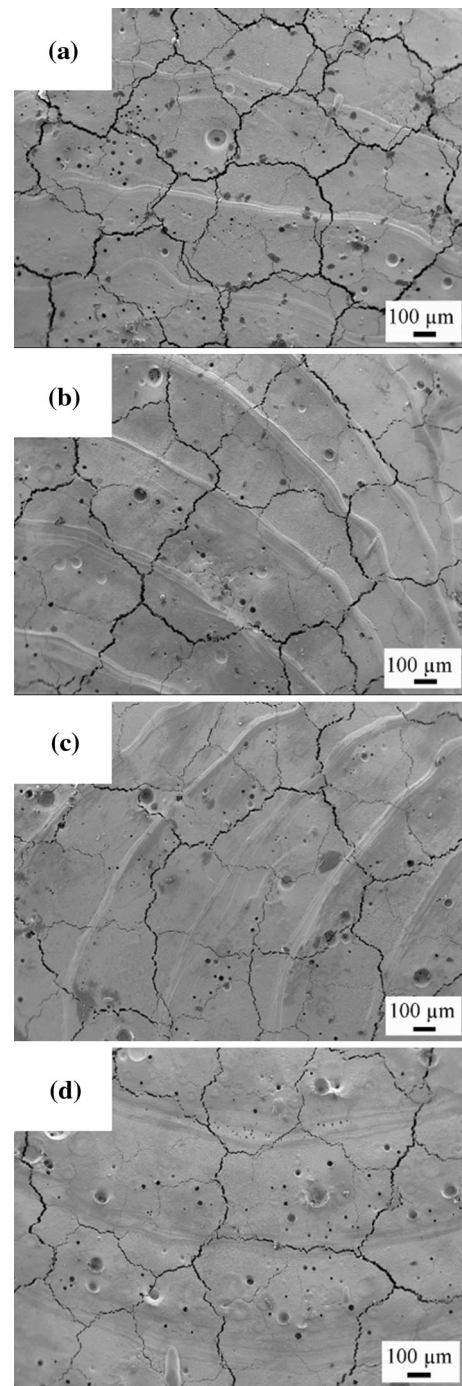
energy density should be also taken into account to estimate the depth of glazed layers marked with different cycles in Fig. 10. It is noticed that the change in scanning speed and energy density does not influence so much the depth of glazed layer. However, depth of glazed layer is
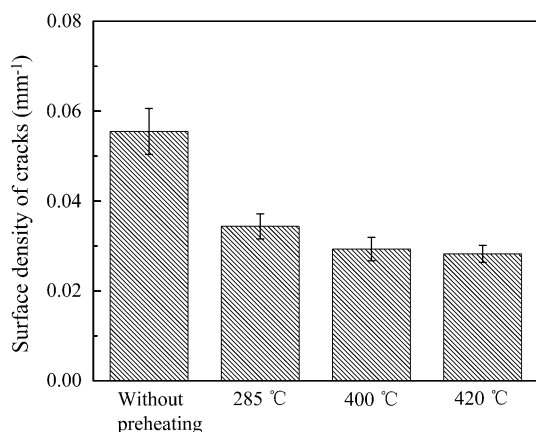
Fig. 7 Surface density of cracks in function of different preheating temperature (0, 285, 400 and 420 °C)
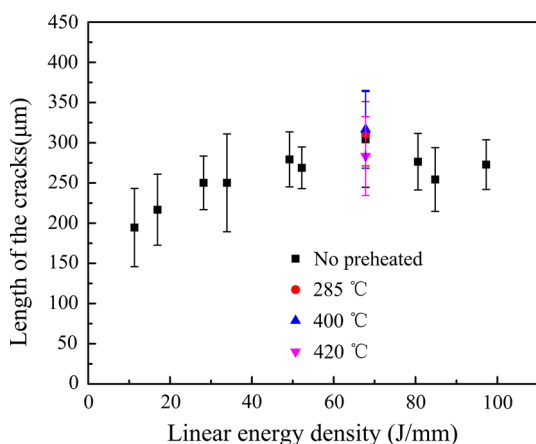

Fig. 8 Length of cracks for different linear energy densities and different parameters of laser-glazing process
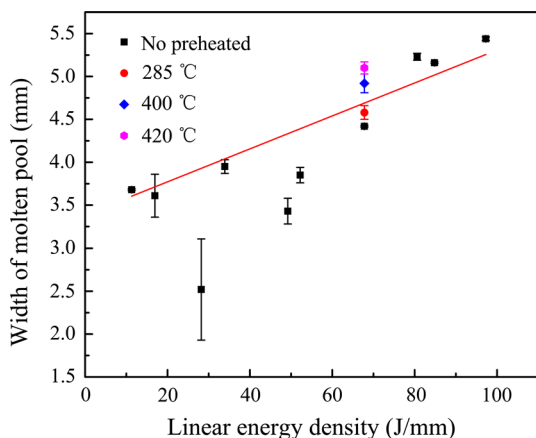

Fig. 9 Width of molten pool for different linear energy densities and different parameters of laser-glazing process

very sensitive to the laser pulse duration. As the duration increases from 3 to 6 ms, the depth of glazed layer increases consequently from 21 to 36 mm. Therefore, the
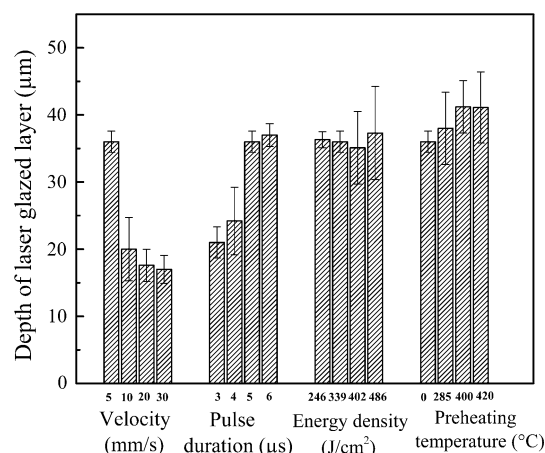

Fig. 10 Depth of glazed layer for different parameters of laser-glazing process

preheating process increases the depth of glazed layer (Fig. 7) as well as it decreases the thermal gradient and cracking in the YSZ coatings.

Conclusions

In this study, various post-laser parameters were investigated on the plasma-sprayed YSZ coating. The result indicates that the laser-glazing process could result in a dense laser-glazed layer, as well as cracks perpendicular and parallel to the coating surface. With the increase in the liner energy density of laser, the width of molten pool increases linearly while the length of cracks maintains constant. It is also found that the depth of the laser-glazed layer is more sensitive to the laser pulse duration compared with the scanning velocity and the power density. Moreover, the influence of the preheating process on the microstructure of laser-glazed coating was investigated intensively, and the result indicates that the preheating process enhances the quality of the laser glazing coatings, since it deepens the glazed layer, widens the molten pool and reduces the cracks.

References

1. G. Antou, G. Montavon, F. Hlawka, A. Cornet, C. Coddet, and F. Machi, Modification of Ceramic Thermal Spray Deposit Microstructures Implementing in Situ Laser Remelting, *Surf. Coat. Technol.*, 2003, **172**(2-3), p 279-290
2. D.E. Wolfe, J. Singh, R.A. Miller, J.I. Eldridge, and D.-M. Zhu, Tailored Microstructure of EB-PVD 8YSZ Thermal Barrier

Coatings with Low Thermal Conductivity and High Thermal Reflectivity for Turbine Applications, *Surf. Coat. Technol.*, 2005, **190**(1), p 132-149

3. D.R. Clarke, M. Oechsner, and N.P. Padture, Thermal-Barrier Coatings for More Efficient Gas-Turbine Engines, *MRS Bull.*, 2012, **37**(10), p 891-898

4. J. Stella, T. Poirier, and M. Pohl, Cavitation-Erosion of 3Y-TZPs Obtained at Different Sintering Temperatures, *Wear*, 2013, **300**(1-2), p 163-168

5. N.Q. Minh and T. Takahashi, *Science and Technology of Ceramic Fuel Cells*, Elsevier, Amsterdam, 1995

6. A.G. Evans, D.R. Mumm, J.W. Hutchinson, G.H. Meier, and F.S. Pettit, Mechanisms Controlling the Durability of Thermal Barrier Coatings, *Prog. Mater Sci.*, 2001, **46**(5), p 505-553

7. K.A. Khor, X.J. Chen, S.H. Chan, and L.G. Yu, Microstructure-Property Modifications in Plasma Sprayed 20 Wt% Yttria Sta-bilized Zirconia Electrolyte by Spark Plasma Sintering (SPS) Technique, *Mater. Sci. Eng. A*, 2004, **366**(1), p 120-126

8. C. Batista, A. Portinha, R.M. Ribeiro, V. Teixeira, M.F. Costa, and C.R. Oliveira, Surface Laser-Glazing of Plasma-Sprayed Thermal Barrier Coatings, *Appl. Surf. Sci.*, 2005, **247**(1-4), p 313-319

9. R. Ahmadi-Pidani, R. Shoja-Razavi, R. Mozafarinia, and H. Jamali, Laser Surface Modification of Plasma Sprayed CYSZ Thermal Barrier Coatings, *Ceram. Int.*, 2013, **39**(3), p 2473-2480

10. C. Batista, A. Portinha, R.M. Ribeiro, V. Teixeira, and C.R. Oliveira, Evaluation of Laser-Glazed Plasma-Sprayed Thermal Barrier Coatings under High Temperature Exposure to Molten Salts, *Surf. Coat. Technol.*, 2006, **200**(24), p 6783-6791

11. C. Batista, A. Portinha, R.M. Ribeiro, V. Teixeira, M.F. Costa, and C.R. Oliveira, Morphological and Microstructural Charac-terization of Laser-Glazed Plasma-Sprayed Thermal Barrier Coatings, *Surf. Coat. Technol.*, 2006, **200**(9), p 2929-2937

12. R. Ahmadi-Pidani, R. Shoja-Razavi, R. Mozafarinia, and H. Jamali, Improving the Thermal Shock Resistance of Plasma Sprayed CYSZ Thermal Barrier Coatings by Laser Surface Modification, *Opt. Lasers Eng.*, 2012, **50**(5), p 780-786

13. P.-C. Tsai and C.-S. Hsu, High Temperature Corrosion Resis-tance and Microstructural Evaluation of Laser-Glazed Plasma-Sprayed Zirconia/MCrAlY Thermal Barrier Coatings, *Surf. Coat. Technol.*, 2004, **183**(1), p 29-34

14. R. Ghasemi, R. Shoja-Razavi, R. Mozafarinia, and H. Jamali, Laser Glazing of Plasma-Sprayed Nanostructured Yttria Stabi-lized Zirconia Thermal Barrier Coatings, *Ceram. Int.*, 2013, **39**(8), p 9483-9490

15. H.L. Tsai and P.C. Tsai, Laser Glazing of Plasma-Sprayed Zir-conia Coatings, *J. Mater. Eng. Perform.*, 1998, **7**(2), p 258-264

16. H.L. Tsai, P.C. Tsai, and D.C. Tu, Characterization of Laser Glazed Plasma Sprayed Yttria Stabilized Zirconia Coatings, *Mater. Sci. Eng. A*, 1993, **161**(1), p 145-155

17. Q. Liu, Y. Danlos, B. Song, B. Zhang, S. Yin, and H. Liao, Effect of High-Temperature Preheating on the Selective Laser Melting of Yttria-Stabilized Zirconia Ceramic, *J. Mater. Process. Tech-nol.*, 2015, **222**, p 61-74